Thermal Fronts and Cross-frontal Heat Flux in the Southern Yellow Sea and the East China Sea

Sunghyea Park and Peter C. Chu

Department of Oceanography, Naval Postgraduate School, Monterey, CA93943, USA

Report Documentation Page

Form Approved
OMB No. 0704-0188

1. REPORT DATE	2. REPORT TYPE	3. DATES COVERED
2008		**00-00-2008 to 00-00-2008**

4. TITLE AND SUBTITLE	5a. CONTRACT NUMBER
Thermal Fronts and Cross-Frontal Heat Flux in the Southen Yellow Sea and the East China Sea	5b. GRANT NUMBER
	5c. PROGRAM ELEMENT NUMBER
6. AUTHOR(S)	5d. PROJECT NUMBER
	5e. TASK NUMBER
	5f. WORK UNIT NUMBER
7. PERFORMING ORGANIZATION NAME(S) AND ADDRESS(ES) **Naval Postgraduate School,Department of Oceanography,Monterey,CA,93943**	8. PERFORMING ORGANIZATION REPORT NUMBER
9. SPONSORING/MONITORING AGENCY NAME(S) AND ADDRESS(ES)	10. SPONSOR/MONITOR'S ACRONYM(S)
	11. SPONSOR/MONITOR'S REPORT NUMBER(S)

12. DISTRIBUTION/AVAILABILITY STATEMENT
Approved for public release; distribution unlimited

13. SUPPLEMENTARY NOTES

14. ABSTRACT

15. SUBJECT TERMS

16. SECURITY CLASSIFICATION OF:			17. LIMITATION OF ABSTRACT	18. NUMBER OF PAGES	19a. NAME OF RESPONSIBLE PERSON
a. REPORT **unclassified**	b. ABSTRACT **unclassified**	c. THIS PAGE **unclassified**	**Same as Report (SAR)**	**56**	

Corresponding author's address

Sunghyea Park

Department of Oceanography, Naval Postgraduate School,

Monterey, CA93943, USA

Tel: 1-831-656-7819 Fax: 1-831-656-3686

Email: spark@nps.edu

Key words: Southern Yellow Sea and East China Sea, AXBT, synoptic thermal front, cross-frontal heat flux, lateral eddy diffusivity

Running title: Thermal Fronts in Yellow/East China Seas

Abstract

Synoptic features in/around thermal fronts and cross-frontal heat fluxes in the southern Yellow Sea and East China Sea (YES) were examined using the data collected from four airborne expendable bathythermograph surveys with horizontal ~35 km and vertical 1 m (from the surface to 400 m deep) spacings. Since the fronts are strongly affected by YES current system, the synoptic thermal features in/around them represent the interaction of currents t with surrounding water masses. These features can not be obtained from climatological data even with frontal analysis. . The identified thermal features are listed as follows: (1) multiple boundaries of cold water, asymmetric thermocline intrusion, locally-split front by homogeneous water of ~18°C, and mergence of the front by the Taiwan Warm Current in/around summertime southern Cheju–Yangtze Front and Tsushima Front; (2) springtime frontal eddy-like feature around Tsushima Front; (3) year-round cyclonic meandering and summertime temperature-inversion at the bottom of the surface mixed layer in Cheju–Tsushima Front; and (4) multi-structure of Kuroshio Front. In Kuroshio Front the mean variance of vertical temperature gradient is an order of degree smaller than that in other YES fronts. The southern Cheju–Yangtze Front and Cheju–Tsushima Front are connected with each other in the

summer with comparable cross-frontal temperature gradient. However, cross-frontal heat flux and lateral eddy diffusivity are stronger in the southern Cheju–Yangtze Front. The cross-frontal heat exchange is the largest in the mixing zone between the modified Yellow Sea Bottom Cold Water and the Tsushima Warm Current, which is attributable to enhanced thermocline intrusions.

1. Introduction

The Yellow Sea and East China Sea (YES) are marginal seas of the western Pacific, bounded by China, Korea, and Japan in the west, north, and east, and reach the Okinawa Trench in the south (Fig. 1). With a border line connecting the Yangtze River mouth and Cheju Island, north of YES is the Yellow Sea (YS), and south the East China Sea (ECS). About 70% of YES is covered with a well-developed continental shelf of a depth shallower than 200 m, and the rest with a deep trench of steep bottom topography. Not only these geographical characteristics but also the Kuroshio intrusion from the south facilitates the occurrence of fronts.

The Yellow Sea has large temporal and spatial thermal variability (Chu *et al.*, 1997a, b). Surface thermal fronts throughout YES have been studied comprehensively using remotely-sensed data since 1970s. Ning *et al.* (1998)

identified five fronts derived from combined AVHRR SST and CZCS-derived pigment concentration data. Hickox *et al.* (2000) produced year-round climatology of ten thermal fronts based on Pathfinder SST (1985-1996). It is however for specific regions that the studies including subsurface thermal frontal features have been done using in situ observations: for instance, along the Kuroshio (Qui *et al.*, 1990; Hsu *et al.*, 1997; Oka and Kawabe, 1998; Yan *et al.*, 2003; Chu *et al.*, 2005), along the Tsushima Warm Current (Guo *et al.*, 1998; Lee *et al.*, 2003), around the Yellow Sea Bottom Cold Water (YSBCW) (Hu, 1994; Tang *et al.*, 2000), around the Cheju Island (Son *et al.*, 2003), and along the southern coast of Korea (Kim and Yug, 1983). However, seldom have studies of subsurface thermal fronts throughout YES been done.

Recently, Park and Chu (2006b, hereafter PC06) identified the thermal and haline fronts at both surface and subsurface throughout YES from a climatological dataset [i.e., Generalized Digital Environmental Model (GDEM)] with three-dimensional distributions and seasonality. Characteristics of the fronts were examined in terms of frontal intensity, water mass distribution, and temporal evolutions of temperature and salinity across the fronts. However, a variety of frontal features such as intrusion, inversion, and evidence of mixing could not be well presented because of inevitable weaknesses of the climatological dataset itself.

There were four airborne expendable bathythermograph (AXBT) surveys with horizontal spacing of 35 km and vertical resolution of 1 m from the surface to 400 m depth, which are invaluable to explore synoptic thermal features throughout the southern YS, ECS, and the southern Japan/East Sea at both surface and subsurface. For YES these surveys cover the region from the deep trench to the shelf as shallow as 50-75 m depth (Fig. 1). Using these AXBT data, Furey and Bower (2005, hereafter FB05) analyzed variability of mixed layer depth, path change of the Kuroshio associated with generation of cold eddies on canyons northeast off Taiwan, and seasonal evolution of thermal fronts in YES and the Japan/East Sea. Park and Chu (2007, 2008) examined characteristics of YES finestructures in temperature profiles, their generation mechanisms, related mixing processes, synoptic features of vertical layers, and the Monin-Obukhov depth.

Here, we explore detail synoptic features in/around thermal fronts in YES, which have not been reported in other studies. These data reveal various synoptic thermal features in/around the fronts; for instance, inversions (temperature increases with depth), multilayers (a temperature profile is vertically fluctuated and then is divided into several layers such as a temperature-inverted layer, an isothermal layer, and so forth), and ragged isotherms (isotherms are "ragged", not smooth, at a vertical scale of few to tens meters) are prominent in/around a front

detected in 127.5°E (Fig. 2). However, these features are not seen in the climatological dataset (e.g. GDEM) at all even though the front is seen in 127.5°E. These synoptic thermal features, like an example in Fig. 2, can reveal how currents interact with surrounding water masses in/around the fronts since the fronts are strongly affected by the YES current system comprising the Kuroshio, the Tsushima Warm Current, the Taiwan Warm Current, and the Cheju Warm Current. In addition, we estimate cross-frontal heat flux and lateral eddy diffusivity in the fronts. Estimates of cross-frontal heat flux can quantify the front-contributed heat exchange with surrounding water masses, which is associated with frontal mixing. The estimates from observation data are useful for validating estimates from numerical simulations. In YES where the fronts are dynamically related to each other by the connected current system, comparison of the cross-frontal heat flux among the fronts can predict the heat loss from the connected current system (only by cross-frontal heat exchange).

The rest of the paper is organized as follows. Section 2 gives a brief description of the AXBT data. Section 3 summaries how to identify the thermal fronts in the data. Section 4 describes the synoptic characteristics of the fronts with their horizontal/vertical distributions and presents plausible explanations on the frontal features in connection with the frontal structures, the water masses, and the

circulation system. Section 5 estimates the cross-frontal heat flux and the lateral eddy diffusivity. Section 6 presents conclusions.

2. AXBT Measurements

The AXBT data consist of 1256 profiles from the four surveys (Fig. 1): 18–29 September 1992 (named as 9209), 4–14 February 1993 (as 9302), 5–14 May 1993 (as 9305), and 2–10 September 1993 (as 9309). The data, a part of the Master Oceanographic Observation Data Set (MOODS), were obtained under the approval by the Naval Oceanographic Office (NAVOCEANO). The data including their detail information have not been open to the public yet. In 1990s, Sparton AXBTs were widely used in U.S. Navy research. Their thermal time constant 0.1 s or less and their vertical resolution is 15 cm (Boyd and Linzell, 1993). We obtained the edited AXBT data with 1 m vertical resolution. The editing process includes the followings: indentifying recording errors and outliers, checking duplicate profiles, checking depth inversion and depth duplication for individual profiles, checking temperature range, checking large temperature inversions and gradients, checking standard deviation, interpolation to standard levels, and post objective analysis checks (Jugan and Beresford, 1992; Boyer and Levitus, 1994; Chu *et al.*, 1997b, 1998). Customized equations, which were achieved using concurrent CTD data,

provide the accuracy of temperature data of 0.13°C and that of depth of ±2% of depth or ±10 m, whichever is greater. The Naval Research Laboratory (NRL) Isis System determines the AXBT frequency to such accuracy that the resulting temperature accuracy is 0.05°C or better (Boyd and Linzell, 1993).

The four surveys almost repeated themselves in track paths with slight mismatch and were completed within one week except for some profiles near the Korea/Tsushima Strait, so that the seasonality of the thermal features in/around the fronts can be identified. The synoptic variability of the thermal features can be identified only for the features with horizontal scales larger than tens kilometer and duration longer than a week.

3. Identification of Fronts

A horizontal temperature gradient is expressed by

$$\Delta T(i) = \sqrt{\left(\frac{\partial T(i)}{\partial x}\right)^2 + \left(\frac{\partial T(i)}{\partial y}\right)^2},$$

where $T(i)$ and i are temperature and spatial index, respectively (PC06). The gradient is calculated at 0 (the sea surface), 25, 50, and 75 m depths (Fig. 3). A thermal front is identified by the horizontal temperature gradient of >5ºC/100 km,

which is close to a criterion (2ºC/35 km) applied by FB05 (see their Fig. 5 for the front schematic at 60m depth) but greater than a criterion (2ºC/100 km) by PC06 because fronts are usually sharper and stronger in in-situ observation than in the climatological dataset (as seen in Fig. 2). The gradient method is also used for satellite data: for instance, 0.50^{o}C/9 km for thermal fronts in the northern South China Sea using NOAA/NASA Pathfinder SST (Wang *et al.*, 2001). The identified thermal fronts are Cheju–Yangtze Front (CYF), Cheju–Tsushima Front (CTF), Tsushima Front (TF), and Kuroshio Front (KF) (Fig. 3); their name and definition are referred to PC06. Their alternative names are in Hickox *et al.* (2000, Fig. 2). FB05 also presented a schematic of fronts at 60 m depth in their Fig. 6. CYF is two-tongue-shaped, northern and southern tongues. CTF occurs along the southern coast of Korea and expands between the Cheju Strait and the Korea/Tsushima Strait. TF is a branch from KF. The southern tongue of CYF migrates southward/southeastward from the winter to the summer (FB05; PC06). In warm seasons the southern tongue of CYF merges to TF and forms one broad front. In comparison with a map of the fronts of the climatological data (PC 06, Fig. 5), the fronts show more spatial variability. Many minor front-like features unseen in the climatological data are located near the four major fronts, which will be explored in this study.

In addition to the horizontal temperature gradient distribution, we will show horizontal temperature distributions at 25 m and 50 m depths and vertical ones along Section-a through Section-f to describe the fronts and related thermal features. The distribution at 25 m depth is suitable to show summertime thermal features induced by bottom cold waters on the shallow shelf. Its February distribution shows the all major thermal fronts in single plot (see the fronts drawn in Fig. 3 and Fig. 4). The distribution at 50 m depth has been frequently seen in many studies to show hydrographic features near the bottom in YES (e.g. Park, 1986; Isobe, 1999; Lie *et al.*, 2000), so that it can be conveniently compared with others although it is similar to the distribution at 60m (FB05, Fig. 4). See FB05 for more horizontal temperature distributions (at 60 m and 100 m depths) and vertical ones (on ECS shelf and Cheju Island to the Korea/Tsushima Strait).

4. Synoptic Features of the Fronts

4.1. Cold Water Masses in the Southern CYF Tongue

In the winter the southern tongue of CYF is viewed as the southward/southeastward invasion of the cold water (9302 in Figs 4, 5). A single cold water mass exists over 29.5-32.5°N with the central temperature of <10°C (Fig. 6-9302). From the winter to the spring, the sharp front still exists below 20 m depth

(see isotherms of 13–16°C around 30°N in Fig. 6-9302, 9305) and is shifted southeastward (Fig. 4-9302, 9305). Multiple cold water masses are generated in the spring and last in the summer with temperature of <10°C (YSBCW), 10–12.5°C, and 13–15°C (9305, 9209, and 9309 in Fig. 6, 7); the last two cold water masses are mixed water (named as modified YSBCW). The modified YSBCW is affected by surface heating, horizontal advection, and degree of mixing, resulting in seasonal change in its volume and location. It is also detected in several studies (Park, 1986; Chen *et al.*, 1994; Isobe, 1999; FB05 (with same data)) with temperature ranging slightly different from this study though.

4.2. Year-to-Year Variability in the Summer CYF and TF

In the summer the northern CYF tongue weakens, and TFstrengthens. The southern CYF tongue connects to CTF at the subsurface instead (FB05 (with same data); PC06). In 9209, isotherms meander with strong temperature gradient from the eastern tip of the Yangtze Bank to the Korea/Tsushima Strait (Fig. 5-9209). Compared to the climatology (PC06), the southern CYF tongue is shifted northward and 3–5°C warmer in the southern YS trough and the Yangtze Bank (Fig. 4-9209). In 9309, on the other hand, isotherms meander less with moderate gradient and 2–3ºC colder than the climatology, and the southern CYF tongue extends farther southeastward (9309 in Figs. 4, 5). These contrast features between the two

summers are attributable to contrast atmospheric forcing, stronger wind in 1992 (weaker wind in 1993) than the normal (Yoo *et al.*, 2004; Park and Chu, 2006a). According to COADS monthly wind data, stronger wind blows generally southwestward/westward in 9209 (Park and Chu, 2007). Consequently, more warm water invades northward by the Ekman transport, leading to thicker surface mixed layer. YSBCW shrinks toward the bottom, and the modified YSBCW does not extend farther southeastward.

4.3. Mergence of Thermal Front by the Taiwan Warm Current in Summer

In the summer two fronts are merged at 125–127°E and 30–31°N (9209 and 9309 in Figs. 4, 5). The northern one is the southern CYF describing a distinct boundary against the modified YSBCW, and the southern one is generated by the Taiwan Warm Current and/or the uplifted Kuroshio northeast off Taiwan according to its temperature range (23–27°C) (Hur *et al.*, 1999). This mergence of the southern front into the southern CYF supports that the Taiwan Warm Current is a source of the Tsushima Warm Current in the summer (Isobe, 1999; Ichikawa and Beardsley, 2002; also presented by FB05). As the volume transport of these warm waters increases from spring to summer, the volume of the mixed water between these warm waters and the cold shelf water increases. This mixed water, a relatively homogeneous water mass of 22–23°C, resides between the two fronts,

generally along the shelf in both summers, but is detected at shallower depth in 9309 (9209 and 9309 in Figs. 4, 5; see 30–31°N in Fig. 6-9309).

4.4. Asymmetric Thermocline Intrusion around the Southern CYF Tongue

Vertically homogenous structure around the southern tongue of CYF in the winter implies strong wind and/or convective mixing prevails over horizontal advection or mixing . In other seasons the isotherms are not vertically uniform around the tongue. Note ragged isotherms are more evident around the eastern side of the tongue (e.g., 127–127.5°E in Fig. 8-9209) than around the western side of the tongue (e.g., ~125.5°N in Fig. 8-9209). This vertical structure that temperature profiles display multilayered or inverted structures at thermocline depths is called thermocline intrusion (Ruddick and Richards, 2003). The western side of the tongue is located on the shallow bank where the bottom tidal mixing is strong, resulting in the lack of ragged isotherms around the tongue.

In the spring the ragged isotherms in the eastern side of the tongue exhibit high possibility of mixing (126–127°E in Fig. 8-9305). In the summer the isotherms in the upper part of the tongue is inclined seaward and shows rich-ragged structures (126–127°E in Fig. 8-9209, 9309), which is attributable to seaward migration of the tongue. On the contrary, the isotherms in the lower part of the

tongue intrude shoreward in relation to the mass compensation and/or the Tsushima Warm Current intrusion into the shelf region.

4.5. Extrusion around the Southern CYF Tongue

The southern CYF tongue and TF are occasionally combined or separated by variations of the colder water between the tongue and the Tsushima Warm Current. In 9209, the two fronts are combined, showing strong frontal intensity along 127°E (Fig. 5-9209). In 9309, however, the two fronts are separated by relatively homogeneous water masse between the fronts (126.5–127.5°E in Fig. 8-9309). In 9305 the fronts are separated as well (127.2–128.2°E in Fig. 8-9305). This separation may be caused by the extrusions of water from the southern tongue (see stars in Fig. 5). The two extrusion features represent different phenomena.

In 9309 the homogeneous water mass of around 18°C splitting locally the combined front of CYF and TF in a horizontal view (Fig. 5-9309) is infiltrated into the thermocline in 127–128°E and eventually assimilated into neighboring thermocline (Fig. 8-9309). This feature looks like the vertical split of TF. The cross-section along 127.5°E shows that TF is split by the presence of the relatively homogenous water at 50–100 m depth (30.5–33°N in Fig. 9-9309). However, the cross-section along 128.2°E shows that this homogenous water is not distinguishable any more (Fig. 10-9309). Meantime, the extrusion feature in 9305

might be associated with a frontal eddy-like feature, which will be explained in section 4.6.

4.6. Frontal Eddy-like Feature around TF

In 9305 TF meanders cyclonically (see the star in Fig. 5-9305), and thus upwelling can be induced in the center of this cyclonic meander. In Fig. 9-9305 cold water (<15°C) is upwelled at 31.3–32°N, right before the shoreward boundary of TF (31°N; KF is in 29–30°N), from the bottom to the near-surface on the shelf-break. This cold water is surrounded by warm water (>18ºC). These horizontal and vertical structures are similar to those of a frontal eddy, which is also seen in Fig. 8-9305 (126.5–128.5°E) and Fig. 10-9305 (31–33°N). Fig. 4-9305 (127–129°E, 31–33°N) also describes a frontal eddy-like feature with isotherms of 18–19°C. Its horizontal scale is ~100 km, compatible to frontal eddies often detected around KF (Qui *et al.*, 1990; Yanagi *et al.*, 1998; James *et al.*, 1999; Isobe *et al.*, 2004); however, a frontal eddy around TF has been seldom reported. Taking bottom topography and occurrence of a strong front (i.e. TF) into account, this region is appropriate to induce the frontal eddy as the Kuroshio region in ECS.

4.7. Meandering of CTF

Year-round CTF is connected to either the northern (winter at all the depth) or the southern (summer at the subsurface) tongue of CYF/TF (PC06). CTF

meanders more in the summer than in the winter (Figs. 4, 5). A cyclonic meandering is marked around 128–129°E and 34–35°N in 9209 (Figs. 4, 5). In the vertical view this cyclonic meandering is identified by a convex thermocline, which is above near-bottom cold water of 14–16ºC (128.2–129.2°E in Fig. 11-9209). This feature suggests that the cyclonic meandering is associated to the near-bottom cold water. The near-bottom cold water of ~14ºC is also detected in the winter and spring (Fig. 11-9302, 9305). Accordingly, the cyclonic meandering could be sustained throughout the season regardless of its spatiotemporal variability. The near-bottom cold water is expected to extend shoreward by Lee *et al.* (1984)'s observation, but its formation and maintaining mechanism are not known. In addition, it needs to be examined whether the near-bottom cold water induces the cyclonic meandering or vice versa.

4.8. Warm-anomaly at the Bottom of Surface Mixed Layer in Summer CTF

In both summers (9209 and 9309) temperature profiles in CTF show existence of warm-anomaly, i.e. inverted structures, describing that maximum temperature is observed between the surface mixed layer and the top of strong thermocline, at 10–50 m depth (see Fig. 3-9209, 9309 in Park and Chu, 2008). The warm-anomaly is ~10 m thick and 0.5–1°C warmer than surroundings. They are found in 127.5–128.5°E and ~129.5°E along section-f, where the isotherms are

concave (Fig. 11-9209). Such a shape of isotherms implies an anticyclonic motion, and downwelling is therefore possible there. The downwelling facilitates downward heat transfer. When stratification in thermocline is extremely strong, a part of downward heat flux does not transfer to the thermocline and thus piles up at the bottom of the surface mixed layer. The temperature near the bottom of the surface mixed layer therefore increases locally, yielding the inverted structure in the temperature profiles, i.e. the warm-anomaly. On the other hand, Kim and Yug (1983) reported a possibility of cold-water in the surface layer of this region in the summer, which might be caused by seaward movement of cold coastal water in the surface layer driven by summer monsoon (southwesterly). Since they presented neither temperature profiles nor a vertical resolution of the data, we cannot compare these inverted structures with theirs. In the AXBT data there is no evidence of the seaward movement of cold coastal water at upper 15 m depth in the region where the inverted structures are detected (not shown). Instead, an anticyclonic meandering of isotherms is found there. These inverted structures are plentiful in 9209 when the anticyclonic meandering are strong (Figs. 5, 11; Fig. 3-9209, 9309 in Park and Chu, 2008). What we explained above could be a possible scenario for these inverted structures although it is difficult to reach a firm conclusion at this moment without supportive observations.

4.9. Multi-structure of the KF

In the summer the KF has a multi-structure, i.e. inner/shoreward and outer/seaward KF, with warm eddies along the Okinawa Trench (see Fig. 6 in FB05, the horizontal temperature distribution at 100m depth resembles that at 75m depth); the horizontal temperature gradient distribution also confirms the multi-structure (see grey thick lines in Fig.3-75 m). The multi-structure is depicted well, for instance, in Fig. 9-9309: the inner KF in ~29.5°N, the warm eddy in ~29°N, and the outer KF in ~28.6°N. The inner KF following a 200 m isobath in Fig 3-75 m is the major one, which forms along the ECS shelf throughout the year. The outer KF, which is in the seaward of the inner KF and generally parallel to it, is most evident in the summer when the warm eddies grow. The outer KF is weaker and more distant from the inner KF in the spring than in the summer. The outer KF is not detected in the winter. Since the outer KF is not as strong as the inner KF, it is hardly detected in the climatological data. Instead, a series of tongue-shaped isotherms represent the existence of warm eddies and the outer KF (PC06). The outer KF is interpreted as the southward return flow of the Kuroshio (Kondo, 1985) or a weak flow along the seaward boundary of the Kuroshio (FB05).

5. Cross-Frontal Heat Flux

5.1. Joyce's Model

A variability caused by intrusion or interleaving on scales of 1-100 m (finestructure) represents a source for smaller scale structure (microstructure) and a mechanism for cross-frontal heat/salt exchange; production of heat flux by cross-frontal advection (i.e. interleaving or intrusion) is balanced by destruction through intensive vertical mixing (Joyce, 1977). The thermocline intrusions often occur around the southern CYF tongue, TF, and CTF (Park and Chu, 2008). Also, haline intrusions might occur concurrently according to in situ observations (Bao *et al.*, 1996; Lee *et al.*, 2003). It is therefore possible to apply Joyce's model (1977) to estimate the cross-frontal heat flux.

The cross-frontal heat flux $-\overline{\tilde{v}\tilde{T}}$ and lateral eddy diffusivity $\overline{A_T^H}$ are expressed by

$$-\overline{\tilde{v}\tilde{T}} = \overline{\tilde{A}_T^V \left(\frac{\partial \tilde{T}}{\partial z}\right)^2} \Big/ \frac{\partial \overline{T}}{\partial y}, \qquad \overline{A_T^H} = \overline{\tilde{A}_T^V \left(\frac{\partial \tilde{T}}{\partial z}\right)^2} \Big/ \left(\frac{\partial \overline{T}}{\partial y}\right)^2, \tag{1}$$

where the tilde indicates finestructure-scale variables, and the overbar denotes averaging on scales larger than finestructure; i.e., $\tilde{v}$ and $\tilde{T}$ are finestructure-scale velocity and temperature, respectively, $\partial\overline{T}/\partial y$ is horizontal cross-frontal temperature gradient averaged over large-scale, $\left(\partial\tilde{T}/\partial z\right)^2$ is variance of vertical finestructure-scale temperature gradient, and $\tilde{A}_T^V$ is vertical Austausch coefficient for heat. Estimates for $\tilde{A}_T^V$ vary by two orders of magnitude, depending on mixing characteristics (Garrett, 1979). Since our knowledge of a precise value for $\tilde{A}_T^V$ is still incomplete, a constant value 10^{-4} m^2/s is assumed for it (Joyce, 1977; Georgi, 1981; Bao *et al.*, 1996). The averaged variance of the vertical temperature gradient $\overline{\left(\partial\tilde{T}/\partial z\right)^2}$ is obtained by integrating temperature gradient spectrum from 4 m to 40 m wavelength. The horizontal cross-frontal temperature gradient is measured using neighboring profiles in consideration for a direction of front.

Four parameters, i.e. the averaged variance of the vertical temperature gradient over depths, the cross-frontal temperature gradient, the cross-frontal heat flux, and the lateral eddy diffusivity, are listed in Tables 1 and 2. Table 1 shows averaged values over stations within grey boxes to compare the parameters among the YES fronts, while Table 2 shows values for individual stations marked by

crosses to examine the parameters across or along a certain front (see Fig. 12 for their locations). If the thermocline intrusion or interleaving is not prominent in the profiles, the values remain blank in Table 1 and Table 2.

5.2. Estimates of Cross-Frontal Heat Flux and Lateral Eddy Diffusivity

In the summer the largest lateral eddy diffusivity exceeding O(10^2 m^2/s) are found south of Cheju, a mixing zone between the modified YSBCW and the Tsushima Warm Current water. The cross-frontal heat flux is also greatest, over O(10^{-2} ºC m/s), there (South of Cheju-9209/9309 in Table 1). A sharp contrast between the two water masses and vertically-sheared advection (Figs. 7, 8) might be responsible for large exchange of heat and probably salt. The summer connected southern CYF/TF–south of Cheju–CTF have roughly equal, strong cross-frontal temperature gradients of 8–9×10^{-5} ºC/m (all 9209/9309 except KF in Table 1). However, the cross-frontal heat flux and the eddy diffusivity in CTF and the southern CYF/TF are roughly half those south of Cheju. This difference is attributable to finestructure characteristics in these frontal zones, strength of cross-frontal currents, and cooling-off/diluting-off extent of the Tsushima Warm Current flowing over the ECS shelf. The mixing zone between the modified YSBCW and the Tsushima Warm Current water is rather shifted southeast in the spring than the

summer, and accordingly the variance, the flux, and the diffusivity are larger in CYF/TF than south of Cheju (CYF/TF-9305 and South of Cheju-9305 in Table 1). The averaged variance and the horizontal temperature gradient are larger in the region where the Tsushima Warm Current branches from the Kuroshio than the Kuroshio region (TF branching and KF in Table 1).

As the profiles in/around TF branching and KF show irregular-staircase structures that consist of alternative sheets (strong temperature gradient in short vertical distance) and layers (almost isothermal layer in rather longer vertical distance), rather than the thermocline intrusion or interleaving (Park and Chu, 2008), the cross-frontal heat flux and the lateral eddy diffusivity were not calculated. The variance of the vertical temperature gradient $O(10^{-4}\ ^{o}C^{2}/m^{2})$ in KF (Table 1) is around ten times lower than that elsewhere in YES and comparable to a value of $3\times10^{-4}\ ^{o}C^{2}/m^{2}$ integrated from 1 m to 100 m wavelength by Bao *et al.* (1996), which was computed at (128.2°E, 28.9°N) using spring-time observational data. They estimated the cross-frontal heat flux (5.5×10^{-4} ºC m/s) and the lateral eddy diffusivity (10.3 m^{2}/s), which are lower than those in the southern CYF tongue, TF, and CTF. In KF those two values might fall on $O(10^{-4}\ ^{o}C$ m/s) and O(1−10 m^{2}/s), respectively. The cross-frontal heat flux estimated here is approximated to that in the Gulf Stream, the Polar Front (Antarctic Circumpolar

Current), the confluence zone of the North Atlantic Deep Water, and the Circumpolar Deep Water, and Meddy Sharon. The lateral eddy diffusivity is approximated to that in Meddy Sharon and the Oyashio Front by Ruddick and Richards (2003, Table 1).

The cross-frontal heat flux and the lateral eddy diffusivity tend to be larger at the shoreward side of the southern CYF/TF than at the center of it (Stn 226>Stn 227, Stn 267>Stn 254 in Table 2), because the variance of the vertical temperature gradient is comparable at both stations but the cross-frontal temperature gradient is stronger at the center of the front. The larger flux and diffusivity are due to the frequent occurrence of thermocline intrusion or interleaving at the shoreward side of the front: the frontal exchange occurs more vigorously at the shoreward side of the front since the water mass at shoreward side takes a leading role in variability of the front (PC06). In the summer, the cross-frontal heat flux and the lateral eddy diffusivity tend to be slightly larger in the northern part than the southern part of the front (Stn 217>Stn 228 >Stn 255 in Table 2-9309), implying that the degree of cross-frontal exchange would be different along the front.

6. Conclusions

We have examined the synoptic features in/around the thermal fronts and cross-frontal heat flux in the southern Yellow Sea and the East China Sea using four AXBT surveys in 1992 and 1993 and presented the plausible interpretations of them. The thermal fronts described by PC06 were detected as well using these data: Cheju–Yangtze Front, Cheju–Tsushima Front, Tsushima Front, and Kuroshio Front. In addition, detail features in/around the thermal fronts, which were not seen in PC06, were discovered. The new results from this study are summarized as follows.

(1) The southern CYF tongue has a variety of features in warm seasons: multiple cold mass boundaries, mergence of the thermal front by the Taiwan Warm Current on the ECS shelf, and poor (rich) thermocline intrusion around its western (eastern) part by strong summer bottom tidal mixing. In spring 1993, a frontal eddy-like feature with a horizontal scale of ~100 km is detected in TF. In summer 1993, the homogeneous water of ~18°C splits the combined front of CYF and TF locally in the horizontal view and infiltrates into the thermocline in 127–128°E in the vertical view.

(2) The cyclonic meandering of CTF is sustained throughout the season regardless of its spatiotemporal variability and related to the near-bottom cold

water of 14–16ºC. In the summer the inverted structures, i.e. warm-anomaly, at the bottom of the surface mixed layer (10–50 m depth) are detected in CTF with the thickness of ~10 m and the temperature range of about 0.5–1°C warmer than surroundings. The downward heat flux by anticyclonic motion might cause this phenomenon.

(3) The multi-structure of KF is distinct when the warm eddies along the Okinawa Trench are developed, whereas the inner KF exists throughout the year.

(4) The cross-frontal heat flux is not equivalent among the YES fronts because of differences in surrounding water masses and finestructure characteristics, even though the YES fronts are related with each other through the connected current system in YES. In KF the variance of the vertical temperature gradient is $O(10^{-4}\ ºC^2/m^2)$, which is around ten times lower than elsewhere in YES. In warm seasons the cross-frontal heat flux and the lateral eddy diffusivity are largest [$O(10^{-2}$ ºC m/s) and $O(10^2\ m^2/s)$, respectively] in the mixing zone between the modified YSBCW and the Tsushima Warm Current, which is formed south of Cheju in the summer but rather shifted southeast in the spring (than summer). The sharp contrast between the two water masses and the vertically-sheared advection might be responsible for this large exchange of heat.

(5) The summer connected CYF/TF and CTF reveals roughly equal cross-frontal temperature gradient, but different cross-frontal heat exchange. The cross-frontal heat exchange is lower in CTF, implying differences of frontal finestructures. The cross-frontal heat flux and the lateral eddy diffusivity tend to be larger at the shoreward side than at the center of the southern CYF/TF , caused by the frequent occurrence of thermocline intrusion or interleaving at the shoreward side of the front.

Acknowledgments

This research was sponsored by the Naval Oceanographic Office, Office of Naval Research, and Naval Postgraduate School.

References

Bao, X.-W., X.-H. Fang, and X.-G. Liu (1996) Thermohaline finestructure and its relation with the water masses and currents system in the northern East China Sea. *Chinese J. of Oceanol. and Limnol.*, **14**(2), 122-128.

Boyd, J.D., and R.S. Linzell (1993) Evaluation of the Sparton tight-tolerance AXBT. *J. Atmos. Oceanic Technol.*, **10**, 892-899.

Boyer, T. P., and S. Levitus (1994) Quality control and processing of historical temperature, salinity, and oxygen data. NOAA Technical Report NESDIS 81.

Chen, C., R. Beardsley, R. Limeburner, and K. Kim (1994) Comparison of winter and summer hydrographic observations in the Yellow and East China Seas and adjacent Kuroshio during 1986. *Cont. Shelf Res.*, **14**, 909–929.

Chu, P.C., S.K. Wells, S.D. Haeger, C. Szczechowski, and M. Carron (1997a) Temporal and spatial scales of the Yellow Sea thermal variability. *J. Geophys. Res.*, **102**(C3), 5655-5668.

Chu, P.C., C.W. Fan, C.J. Lozano, and J. Kerling (1998) An airborne expandable bathythermograph survey of the South China Sea, May 1995. *J. Geophys. Res.*, **103**, 21637-21652.

Chu, P.C., C.R. Fralick, S.D. Haeger, and M.J. Carron (1997b) A parametric model for Yellow Sea thermal variability. *J. Geophys. Res.*, **102**(C3), 10499-10508.

Chu, P.C., Y.C. Chen, and A. Kuninaka (2005) Seasonal variability of the East China/Yellow Sea surface buoyancy flux and thermohaline structure. *Adv. Atmos. Sci.*, **22**, 1-20.

Du, Y., Y. Qi, J. Chen, P. Shi, and P. Chu (2003) Sea current observation during ASIAEX East China Sea planning. *Ocean Engineering*, **21** (1), 94–100. (in Chinese with English abstract).

Furey, H., and A. Bower (2005) The synoptic Temperature Structure of the East China and southeastern Japan/East Seas. *Deep Sea Res.II*, **52**, 1421-1442.

Garrett, C. (1979) Mixing in the ocean interior. *Dyn. Atmos. Oceans*, **3**, 239−265.

Georgi., D. T. (1981) On the relationship between the large-scale property variations and fine structure in the Circumpolar Deep Water. *J. Geophys. Res*., **86**, 6556-6566.

Guo, B., H.-J. Lie, J. H. Lee (1998) Interaction of the Kuroshio and shelf water in the Tsushima Warm Current region in summer, *Acta Oceanologica Sinica*, **20** (5), 1−12.

Hickox, R., I.M. Belkin, P. Cornillon, and Z. Shan (2000) Climatology and seasonal variability of ocean fronts in the East China, Yellow and Bohai Seas from satellite SST data. *Geophys. Res. Lett.*, **27**(18), 2945-2948.

Hsu, M.-K., L. M. Mitnik, J.-H. Hu, and C.-T. Liu (1997) Kuroshio front and oceanic phenomena near Taiwan on ERS SAR images. *Proceeding of the 3rd ERS Symposium: Space at the service of our Environment*, pp.17-21, Florence, Italy.

Hu, D.-X. (1994) Some striking features of circulation in Huanghai Sea and East China Sea. in *Oceanology of China Seas (I)*, edited by D. Zhou, Y.-B. Liang, and C. K. Tseng, pp.27-38, Kluwer Academic Publishers, Netherlands.

Hur, H. B., G. A. Jacobs, and W. J. Teague (1999) Monthly variations of water masses in the Yellow and East China Seas. *J. Oceanogr.*, **55**(2), 171-184.

1 Ichikawa, H., and R. C. Beardsley (2002) Review: The Current System in the Yellow and East
2 China Seas. *J. Oceanogr.*, **58**(1), 77–92.
3 Isobe, A. (1999) The Taiwan-Tsushima Warm Current system: its path and the transformation of
4 the water mass in the East China Sea. *J. Oceanogr.*, **55**(2), 185–195.
5 Isobe, A, E. Fujiwara, P.-H. Chang, K. Sugimatsu, M. Shimizu, T. Matsuno, and A. Manda
6 (2004) Intrusion of less saline shelf water into the Kuroshio subsurface layer in the East
7 China Sea. *J. Oceanogr.*, **60**(5), 853-863.
8 James, C., M. Wimbush, and H. Ichikawa (1999) Kuroshio meanders in the East China Sea. *J.*
9 *Phys. Oceanogr.*, **29**, 259–272.
10 Joyce, T. M. (1977) A note on the lateral mixing of water masses. *J. of Phys. Oceanogr.*, **7**, 626-
11 629.
12 Jugan, M.J., and H. Beresford (1992) Editing approach for the Navy's Master Oceanographic
13 Observation Data Set. *Proceed. of MTS '91, An Ocean Cooperative: Industry,*
14 *Government, and Academia*. 1164.
15 Kim, H.-J., and S.-S Yug (1983) Inversion phenomena of temperature in the Southern Sea of
16 Korea. *Bull. Korean Fish. Soc.*, **16**(2), 111-116 (in Korean with English abstract).
17 Kondo, M. (1985) Oceanographic investigations of fishing grounds in the East China Sea and the
18 Yellow Sea–I. Characteristics of the mean temperature and salinity distributions
19 measured at 50m and near the bottom. *Bull. of Seikai Region Fish. Res. Lab.*, **62**, 19–55
20 (in Japanese with English abstract).
21 Lee, J.-C., J.-Y. Na, and S.-D. Chang (1984) Thermohaline structure of the shelf front in the
22 Korea Strait in early winter. *J. Korean Soc. Oceanogr.*, **19**(1), 56-67.

Lee, J.-H., H.-J. Lie, and C.-H. Cho (2003) The structure of ocean fronts in the East China Sea. in *Proceedings of the 12th PAMS/JECSS Workshop*, Hangzhou, China. 2-10-1~2.

Lie, H.-J., C.-H. Cho, J.-H. Lee, S. Lee, and Y. Tang (2000): Seasonal Variation of the Cheju Warm Current in the Northern East China Sea. *J. Oceanogr.*, **56**(2), 197-211.

Ning, X., Z. Liu, Y. Cai, M. Fang, and F. Chai (1998) Physicobiological oceanographic remote sensing of the East China Sea: Satellite and in situ observations. *J. Geophys. Res.*, **103**(C10), 21623-21635.

Oka, E., and M. Kawabe (1998) Characteristics of variations of water properties and density structure around the Kuroshio in the East China Sea. *J. Oceanogr.* , **54**, 605-617.

Park, S. and P. C. Chu (2008) Characteristics of thermal finestructures in the southern Yellow and East China Seas from airborne expendable bathythermograph measurements. *J. Oceanogr.*, accepted.

Park, S., and P. C. Chu (2006a) Interannual SST variability in the Japan/East Sea and relationship with environmental variables. *J. Oceanogr.*, **62**(2), 115-132.

Park, S., and P. C. Chu (2006b) Thermal and haline fronts in the Yellow/East China Seas: surface and subsurface seasonality comparison. *J. Oceanogr*., **62**(5), 617–638.

Park, S., and P. C. Chu (2007) Synoptic distributions of thermal surface mixed layer and thermocline in the southern Yellow and East China Seas. *J. Oceanogr*., **63** (6), 1021−1028.

Park, Y. H. (1986) Water characteristics and movements of the Yellow Sea Warm Current in summer. *Prog. in Oceanogr.*, **17**, 243-254.

Qui. B., T. Toda, and N. Imasato (1990) On Kuroshio front fluctuations in the East China Sea using satellite and in situ observational data. *J. of Geophys. Res.*, **95**(C10), 18191-18204.

Ruddick, B., and K. Richards (2003) Oceanic thermohaline intrusions: Observations. *Prog. in Oceanogr.*, **56**, 499–527.

Son, Y.-T., S.-H. Lee, J. C. Lee, and J.-C. Kim (2003) Water masses and frontal structures in winter in the northern East China Sea. *J. of Korean Soc. of Oceanogr. (The Sea)*, **8**(3), 327–339 (in Korean with English abstract).

Tang. Y., E. Zou, H.-J. Lie, J. H. Lee (2000) Some feature of circulation in the southern Huanghai Sea. *Acta Oceanologica Sinica*, **22** (1), 1−16.

Wang, D., Y. Liu, Y. Qi, P. Shi (2001) Seasonal variability of thermal fronts in the northern South China Sea from satellite data. *Geophys. Res. Lett.*, **28**, 3963−3966.

Yanagi, T., Shimizu, T., and Lie, H.-J. (1998) Detailed structure of the Kuroshio frontal eddy along the shelf edge of the East China Sea. *Cont. Shelf Res.*, **18**, 1039-1056.

Yoo, S.-H., C.-H. Ho, S. Yang, H.-J. Choi, and J.-G. Jhun (2004) Influences of tropical-western and extratropical Pacific SSTs on the East and Southeast Asian climate in the summers of 1993-94. *J. Climate*, **17**(13), 2673-2687.

Figure Captions

Figure 1. Four airborne expendable bathythermograph (AXBT) surveys conducted on 18–29 September 1992 (9209), 4–14 February 1993 (9302), 5–14 May 1993 (9305) and 2–10 September 1993 (9309). Six sections (section-a through section-f) are used to describe the vertical temperature distributions. Contours indicate the bathymetry shallower than 1000 m, and the isobath of 200 m is highlighted by a thick black line.

Figure 2. Comparison of vertical temperature distributions along 31.3°N between AXBT (a) and GDEM (b). Downward pointing triangles mark locations of AXBT deployments.

Figure 3. Horizontal distributions of temperature gradient at 0, 25, 50, 75 m depths. Contour interval is 2.5ºC/100 km, and the contour of >10ºC/100 km is omitted. Considered the horizontal temperature distribution as well (Fig. 4, 5), fronts such as Cheju-Yangtze Front (CYF), Cheju-Tsushima Front (CTF), Tsushima Front (TF), and Kuroshio Front (KF) are depicted by grey thick lines in 9302-25 m. A part of TF, where the gradient is not as strong as 2.5ºC/100 km but TF is thought to be, is marked darker. The distribution at 75m shows a multi-structure of KF by the thick grey lines (see section 4.9). The isobath of 200 m is highlighted by the thick black line.

Figure 4. Horizontal temperature distributions at 25 m depth showing the thermal fronts. The isobath of 200 m is highlighted by the thick black line. Crosses mark locations of AXBT deployments.

Figure 5. As Fig. 4 except for 50 m depth. Temperature is shaded for the profiles extending to deeper 50m depth. The star symbols are explained in the text.

Figure 6. Vertical temperature distributions along section-a (see Fig. 1). Downward pointing triangles mark locations of AXBT deployments. The locations of northern tongue of CYF (n-CYF), southern tongue of CYF (s-CYF), and KF are marked with brackets.

Figure 7. Same as Fig. 6 except for section-b.

Figure 8. Same as Fig. 6 except for section-c.

Figure 9. Same as Fig. 6 except for section-d.

Figure 10. Same as Fig. 6 except for section-e.

Figure 11. Same as Fig. 6 except for section-f.

Figure 12. AXBT stations for calculating vertically-averaged variance of vertical temperature gradient, cross-frontal temperature gradient, heat flux, and eddy diffusivity. Five grey boxes are labeled by B1 (CTF), B2 (south of Cheju), B3 (CYF/TF), B4 (TF branching), and B5 (KF). Box-averaged estimates of the four parameters are listed in Table 1, and estimates of the parameters for individual stations marked with crosses and numbers in Table 2.

Table Captions

Table 1. Estimates of averaged variance of vertical temperature gradient (VTG; $^{o}C^{2}/m^{2}$), cross-frontal temperature gradient (HTG; $^{o}C/m$), cross-frontal heat flux (HF; ^{o}C m/s), and lateral eddy diffusivity (ED; m^{2}/s) that are averaged over the each grey box (see Fig. 12 for the location). HF and ED were not estimated for the profiles in which the thermocline intrusion or interleaving was not prominent.

Table 2. Estimates of averaged variance of vertical temperature gradient (VTG; $^{o}C^{2}/m^{2}$), cross-frontal temperature gradient (HTG; $^{o}C/m$), cross-frontal heat flux (HF; ^{o}C m/s), and lateral eddy diffusivity (ED; m^{2}/s) at stations marked with crosses and numbers in Fig. 12.

Table 1. Estimates of averaged variance of vertical temperature gradient (VTG; $^{o}C^{2}/m^{2}$), cross-frontal temperature gradient (HTG; $^{o}C/m$), cross-frontal heat flux (HF; ^{o}C m/s), and lateral eddy diffusivity (ED; m^{2}/s) that are averaged over the each grey box (see Fig. 12 for the location). HF and ED were not estimated for the profiles in which the thermocline intrusion or interleaving was not prominent.

	VTG	HTG	HF	ED
B1 (CTF-9209/9309)	6.15×10^{-3}	9.14×10^{-5}	6.74×10^{-3}	7.37×10^{1}
B1 (CTF-9305)	2.34×10^{-4}	6.49×10^{-5}	3.65×10^{-4}	5.62×10^{0}
B2 (South of Cheju-9209/9309)	9.85×10^{-3}	8.26×10^{-5}	1.19×10^{-2}	1.44×10^{2}
B2 (South of Cheju-9305)	3.78×10^{-4}	3.83×10^{-5}	9.87×10^{-4}	2.57×10^{1}
B3 (CYF/TF-9209/9309)	5.07×10^{-3}	8.35×10^{-5}	6.07×10^{-3}	7.27×10^{1}
B3 (CYF/TF-9305)	3.10×10^{-3}	5.11×10^{-5}	6.07×10^{-3}	1.19×10^{2}

B4 (TF branching - 9209/9309)	1.10×10^{-3}	8.11×10^{-5}		
B4 (TF branching -9305)	2.66×10^{-4}	8.36×10^{-5}		
B5 (KF-9209/9309)	3.43×10^{-4}	4.58×10^{-5}		
B5 (KF-9305)	2.57×10^{-4}	3.76×10^{-5}		

1

2

Table 2. Estimates of averaged variance of vertical temperature gradient (VTG; $^{o}C^{2}/m^{2}$), cross-frontal temperature gradient (HTG; $^{o}C/m$), cross-frontal heat flux (HF; ^{o}C m/s), and lateral eddy diffusivity (ED; m^{2}/s) at stations marked with crosses and numbers in Fig. 12.

Stations	9209	9305	9309
VTG/226	2.83×10^{-3}		
HTG/226	1.00×10^{-4}		
HF/226	2.83×10^{-3}		
ED/226	2.83×10^{1}		
227	2.77×10^{-3}		
	1.70×10^{-4}		
	1.62×10^{-3}		
	9.52×10^{0}		
267		8.29×10^{-3}	

		7.96×10^{-5} 1.04×10^{-2} 1.31×10^{2}	
254		9.31×10^{-3} 1.02×10^{-4} 9.16×10^{-3} 9.01×10^{1}	
217			2.12×10^{-2} 8.65×10^{-5} 2.45×10^{-2} 2.84×10^{2}
228		8.04×10^{-4} 2.62×10^{-5}	3.77×10^{-3} 1.46×10^{-4}

		3.07×10^{-3} 1.72×10^{2}	2.58×10^{-3} 1.76×10^{1}
255		4.36×10^{-4} 4.80×10^{-5} 9.02×10^{-4} 1.89×10^{1}	9.46×10^{-4} 2.30×10^{-4} 4.12×10^{-4} 1.79×10^{0}

1

2

3

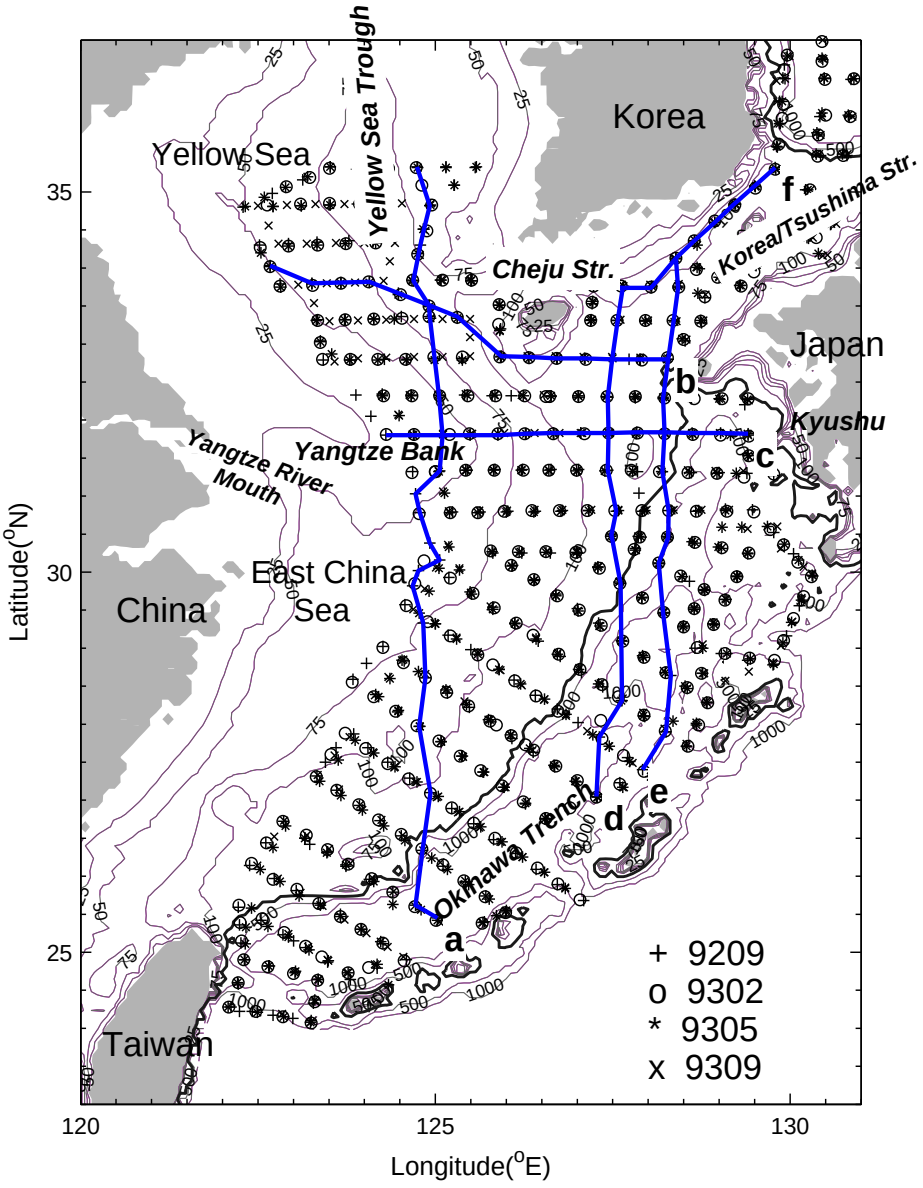

Figure 1. Four airborne expendable bathythermograph (AXBT) surveys conducted on 18–29 September 1992 (9209), 4–14 February 1993 (9302), 5–14 May 1993 (9305) and 2–10 September 1993 (9309). Six sections (section-a through section-f) are used to describe the vertical temperature distributions. Contours indicate the bathymetry shallower than 1000 m, and the isobath of 200 m is highlighted by a thick black line.

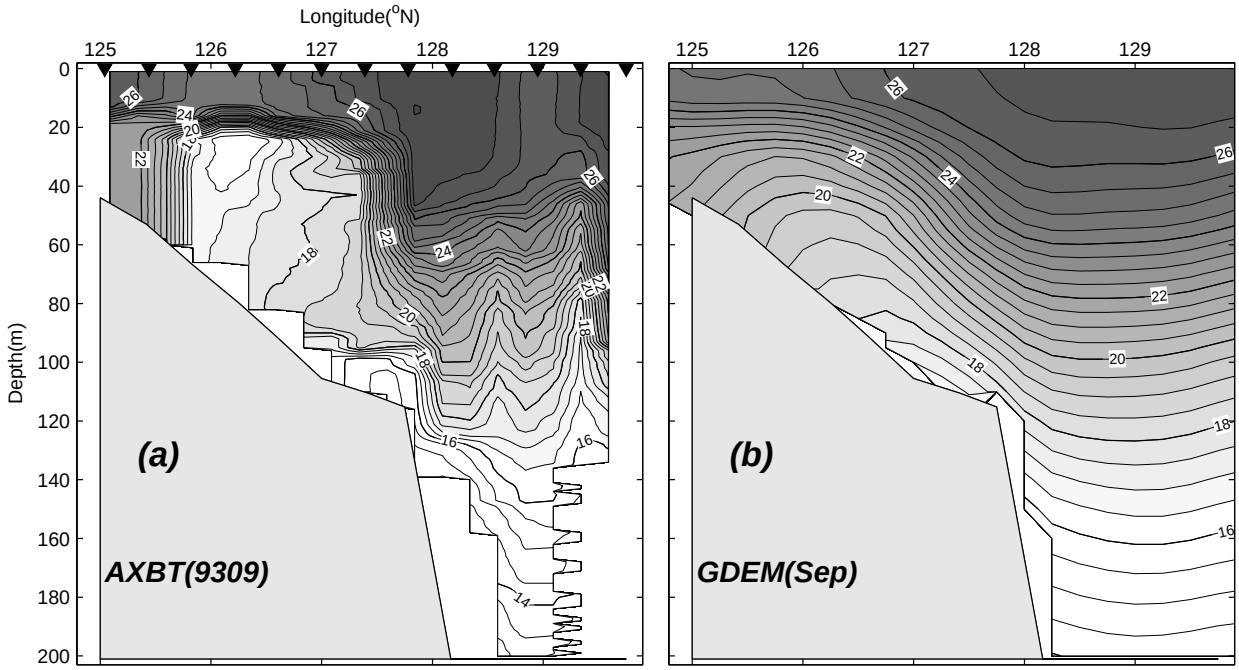

Figure 2. Comparison of vertical temperature distributions along 31.3°N between AXBT (a) and GDEM (b). Downward pointing triangles mark locations of AXBT deployments.

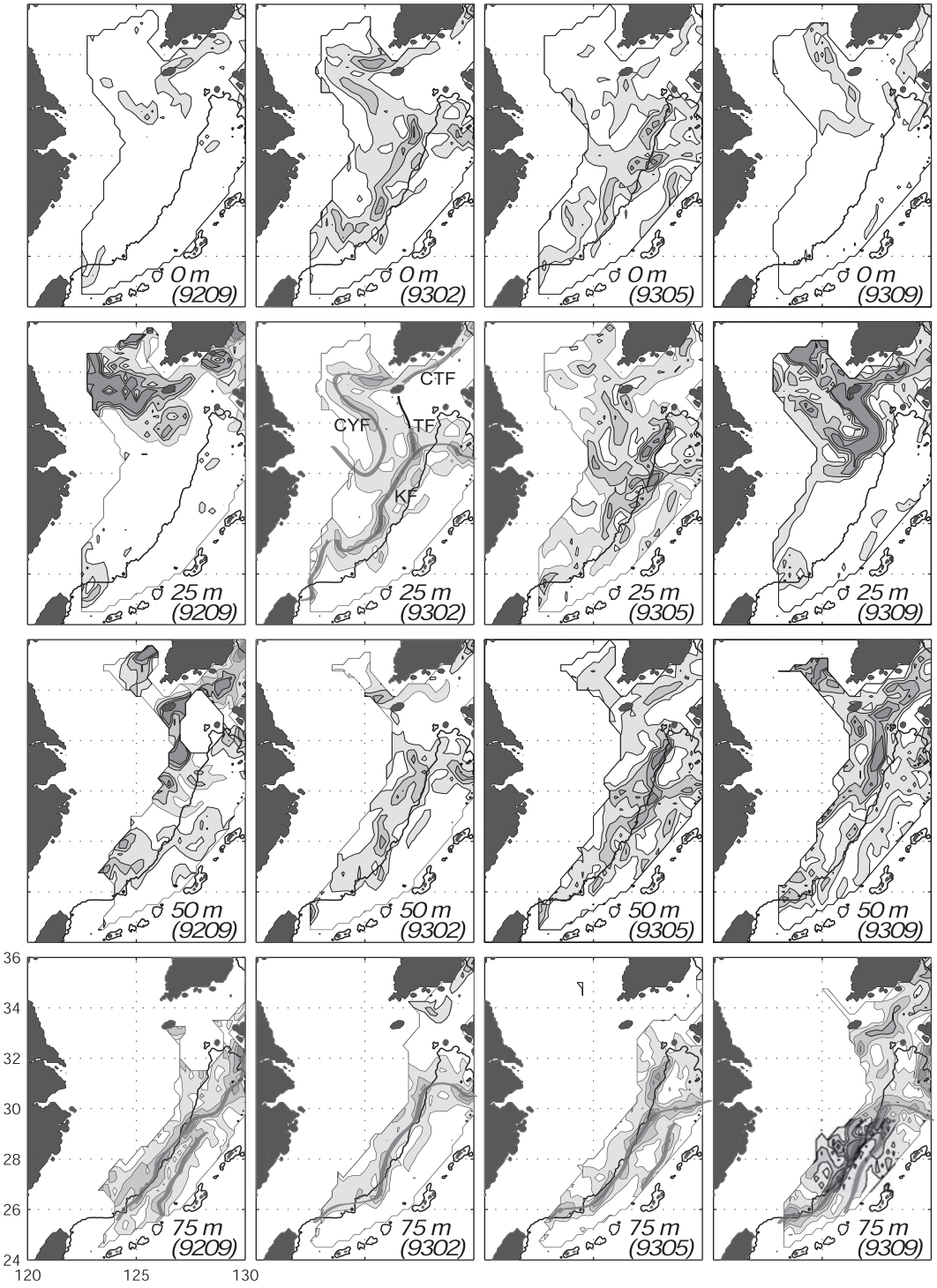

Figure 3. Horizontal distributions of temperature gradient at 0, 25, 50, 75 m depths. Contour interval is 2.5ºC/100 km and the contour of >10ºC/100 km is omitted. Considered the horizontal temperature distribution as well (Fig. 4), fronts such as Cheju-Yangtze Front (CYF), Cheju-Tsushima Front (CTF), Tsushima Front (TF), and Kuroshio Front (KF) are depicted by thick grey lines in 9302-25 m. A part of TF, where the gradient is not as strong as 2.5ºC/100 km but TF is thought to be, is marked darker. The distribution at 75m shows a multi-

structure of KF by the thick grey lines (see section 4.9). The isobath of 200 m is highlighted by the thick black line.

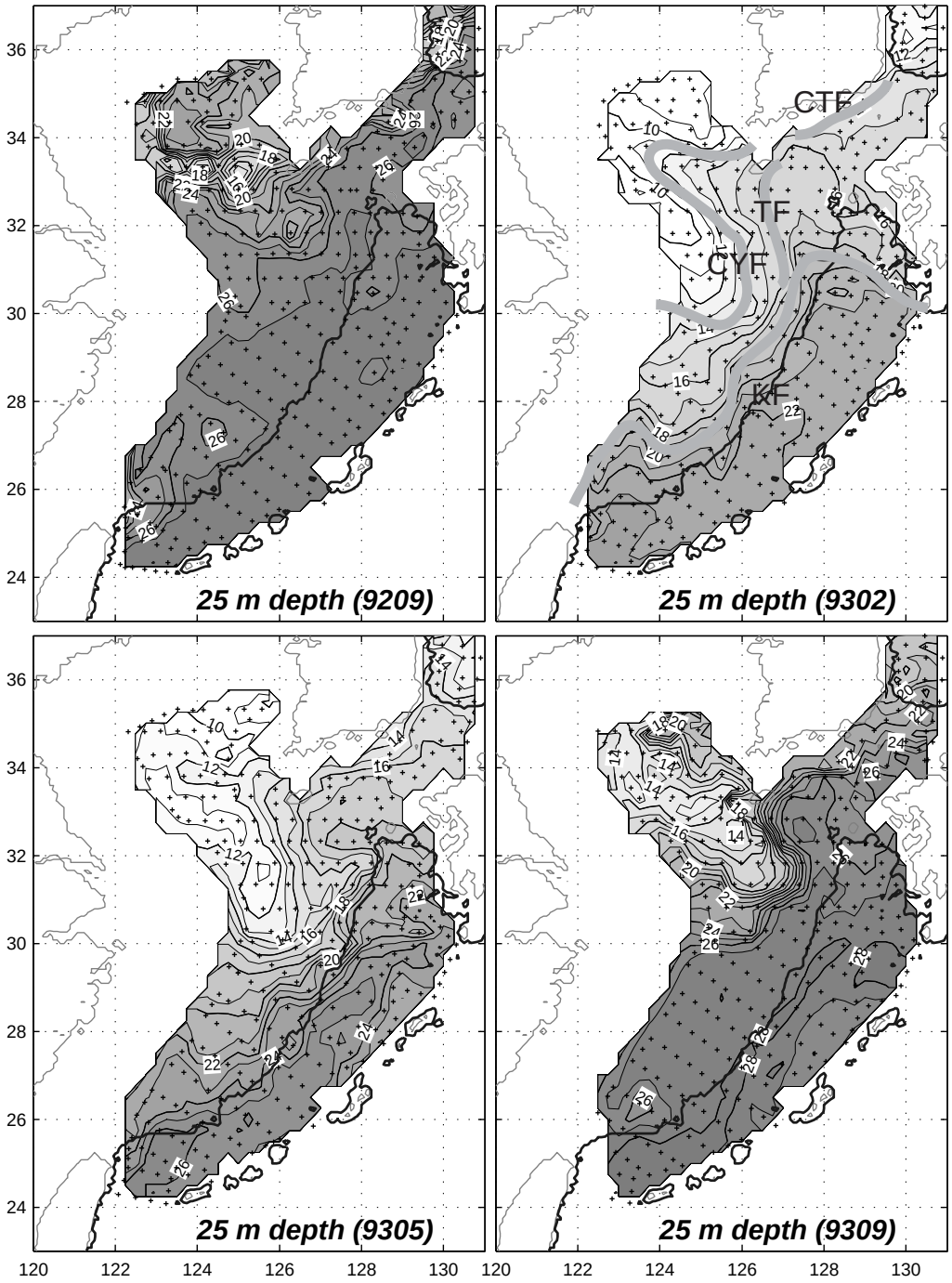
25 m depth (9209)
25 m depth (9302)
25 m depth (9305)
25 m depth (9309)
CTF
TF
CYF
KF
36
34
32
30
28
26
24
120
122
124
126
128
130

1

Figure 4. Horizontal temperature distributions at 25 m depth showing the fronts. The isobath of 200 m is highlighted by a thick black line. Crosses mark locations of AXBT deployments.

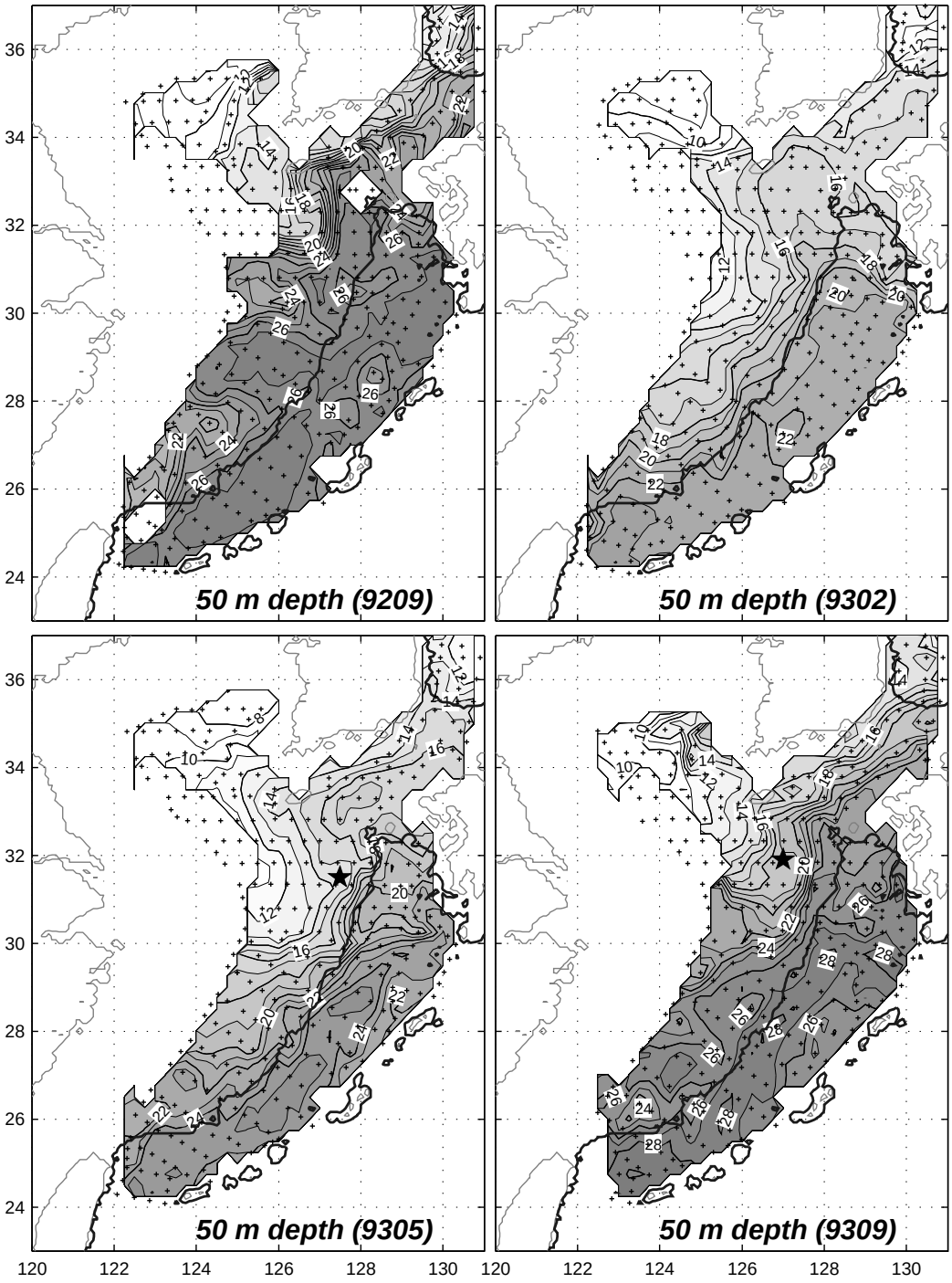
50 m depth (9209)
50 m depth (9302)
50 m depth (9305)
50 m depth (9309)
36
34
32
30
28
26
24
120
122
124
126
128
130

Figure 5. As Fig. 4 except for 50 m depth. Temperature is shaded for the profiles extending to deeper 50m depth. The star symbols are explained in the text.

1

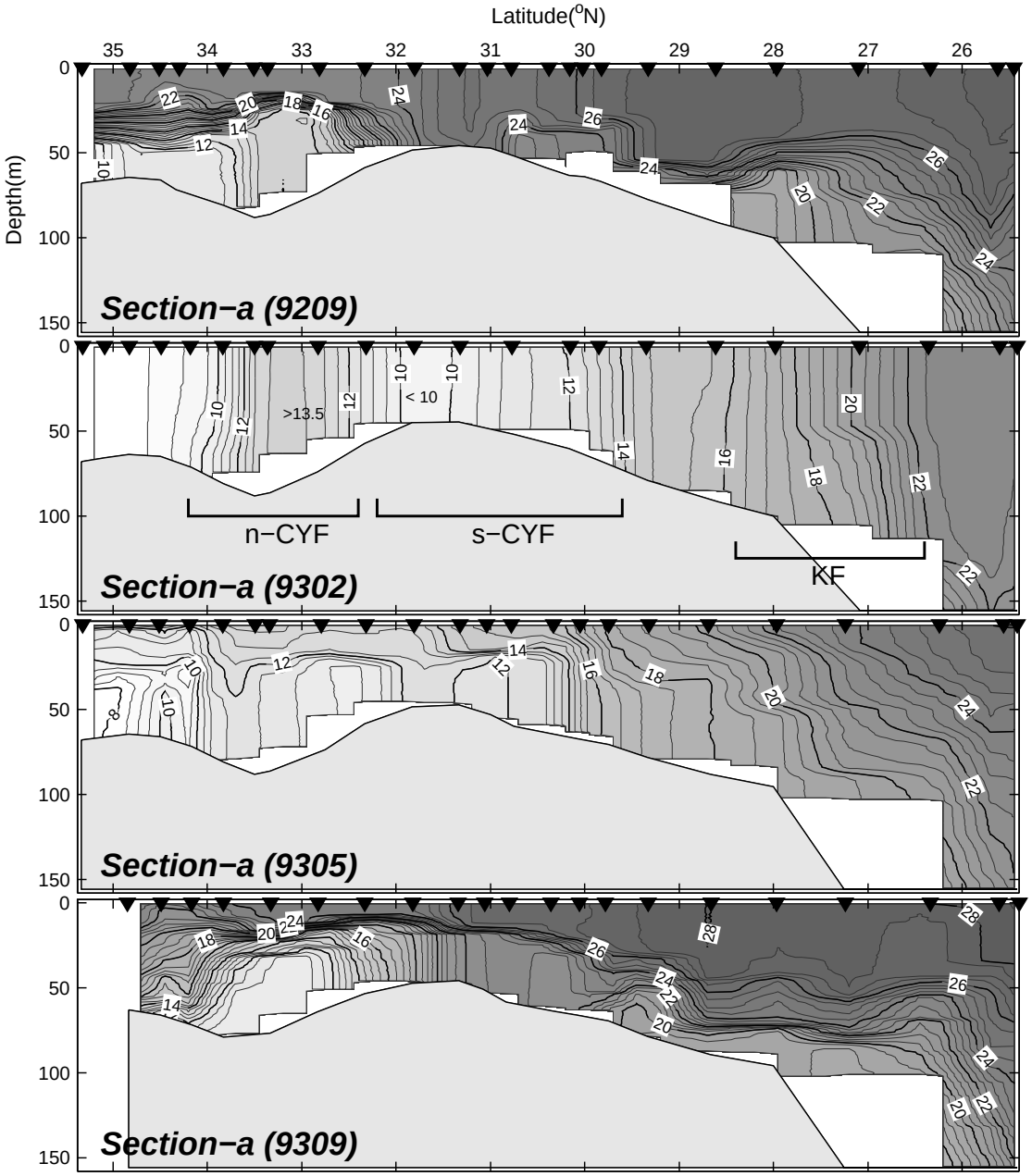
Latitude(0N)
35
34
33
32
31
30
29
28
27
26
Depth(m)
0
50
100
150
Section−a (9209)
Section−a (9302)
Section−a (9305)
Section−a (9309)
>13.5
< 10
n−CYF
s−CYF
KF

2

Figure 6. Vertical temperature distributions along section-a (see Fig. 1). Downward pointing triangles mark locations of AXBT deployments. The locations of northern tongue of CYF (n-CYF), southern tongue of CYF (s-CYF), and KF are marked with brackets.

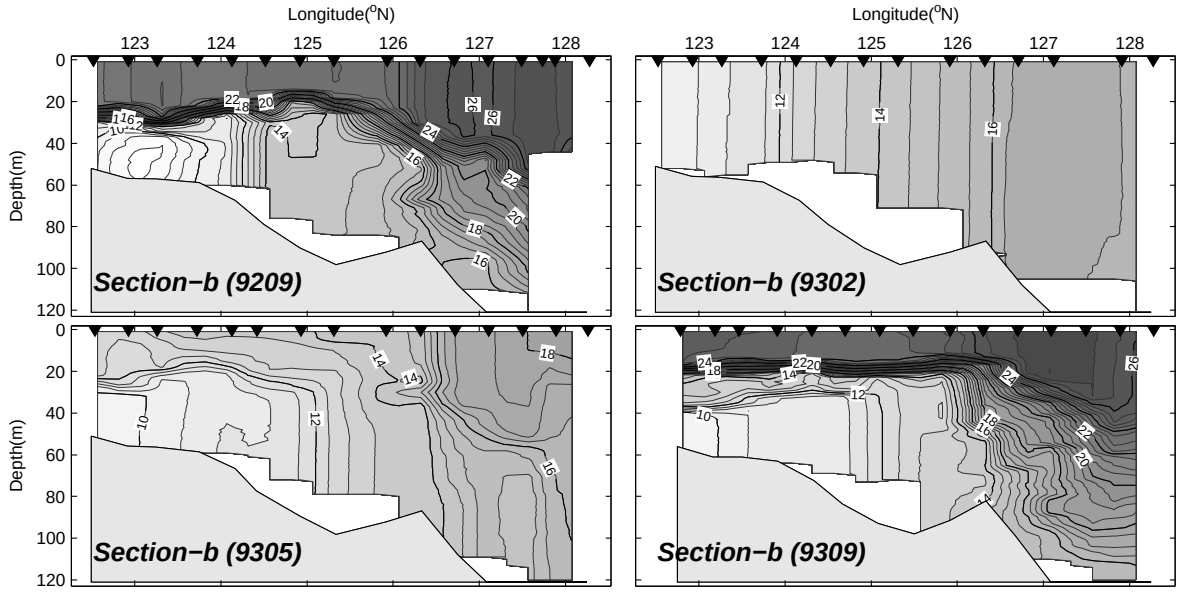

Figure 7. As Fig. 6 except for section-b.

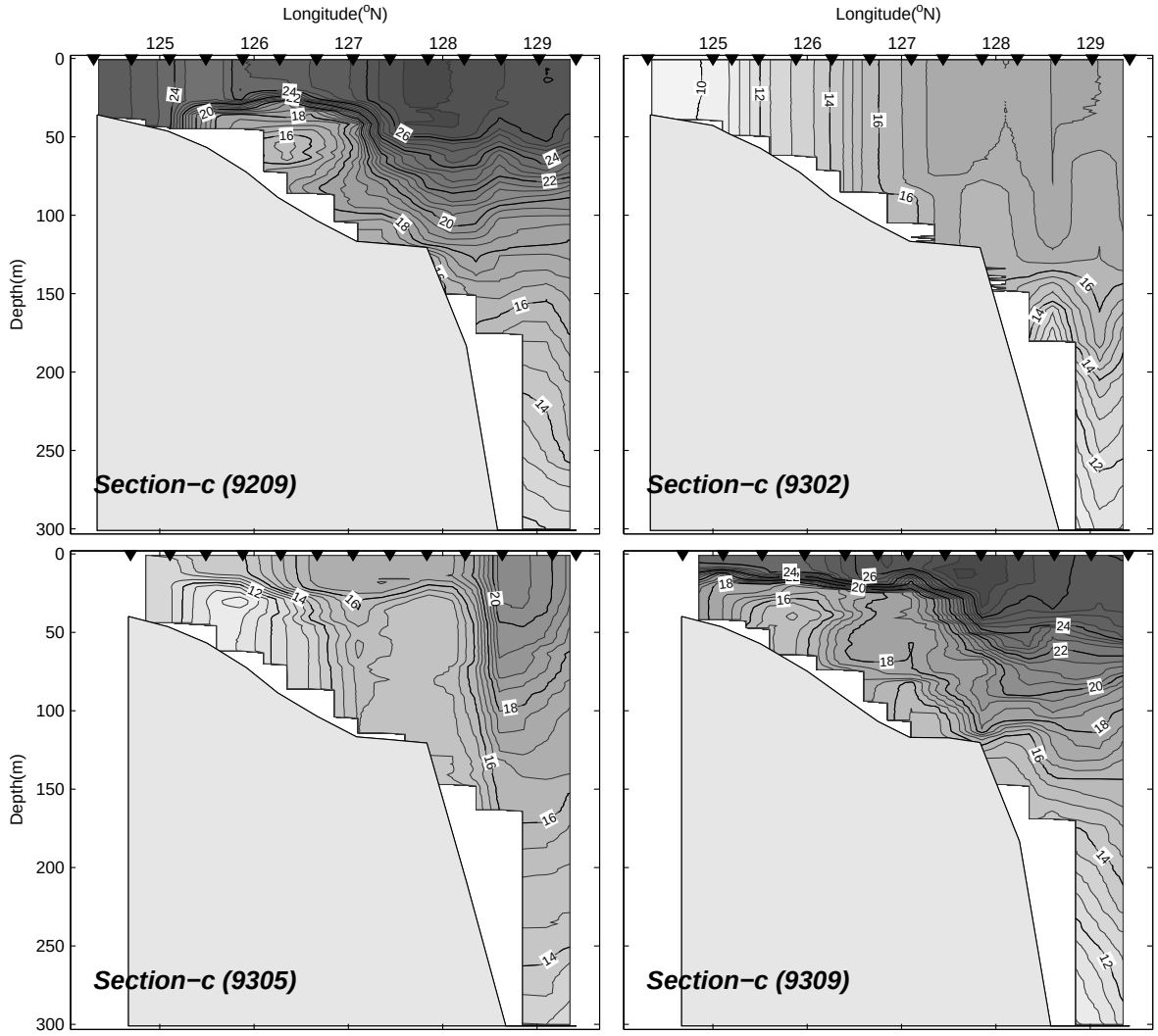

Figure 8. As Fig. 6 except for section-c.

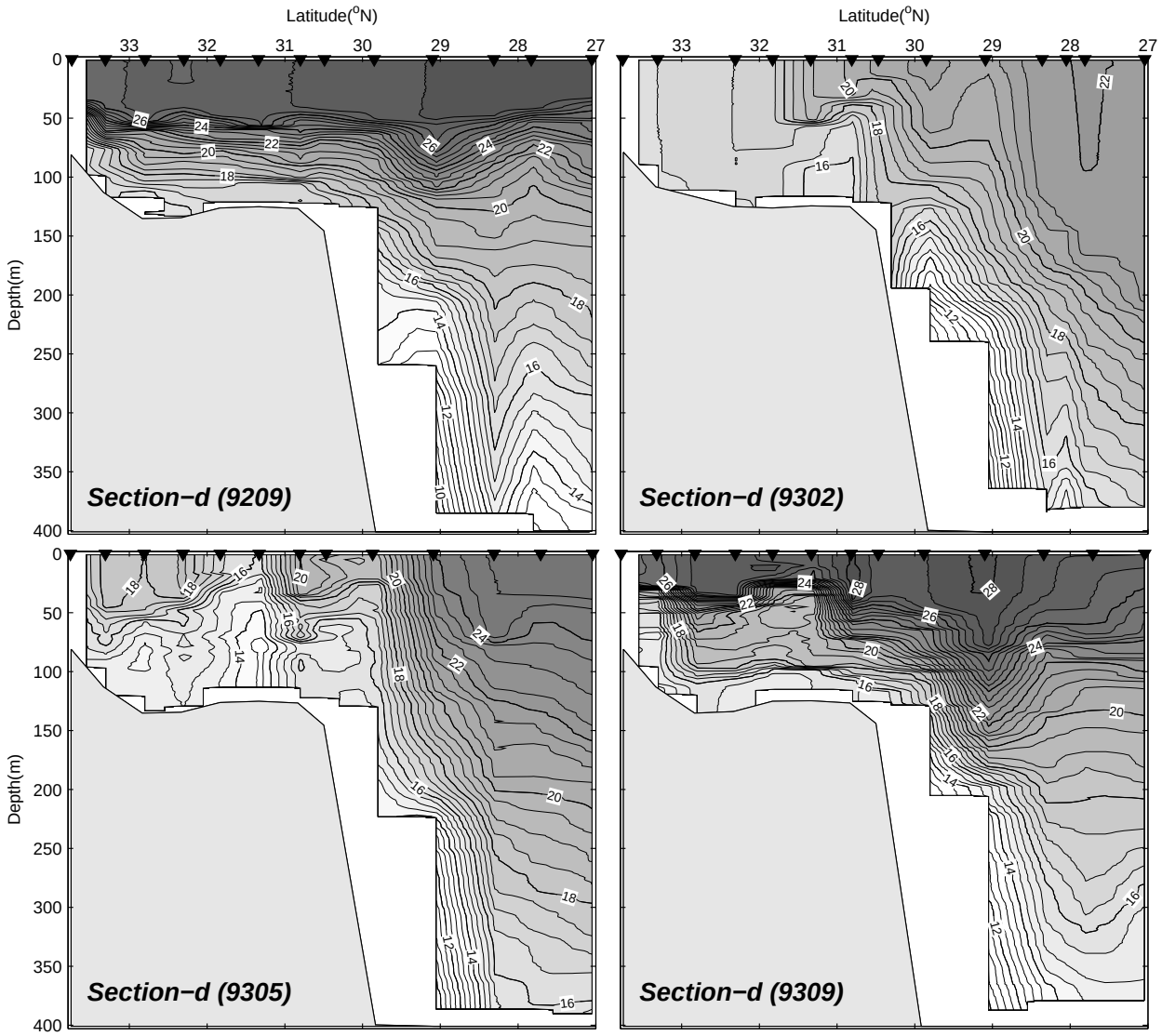

Figure 9. As Fig. 6 except for section-d.

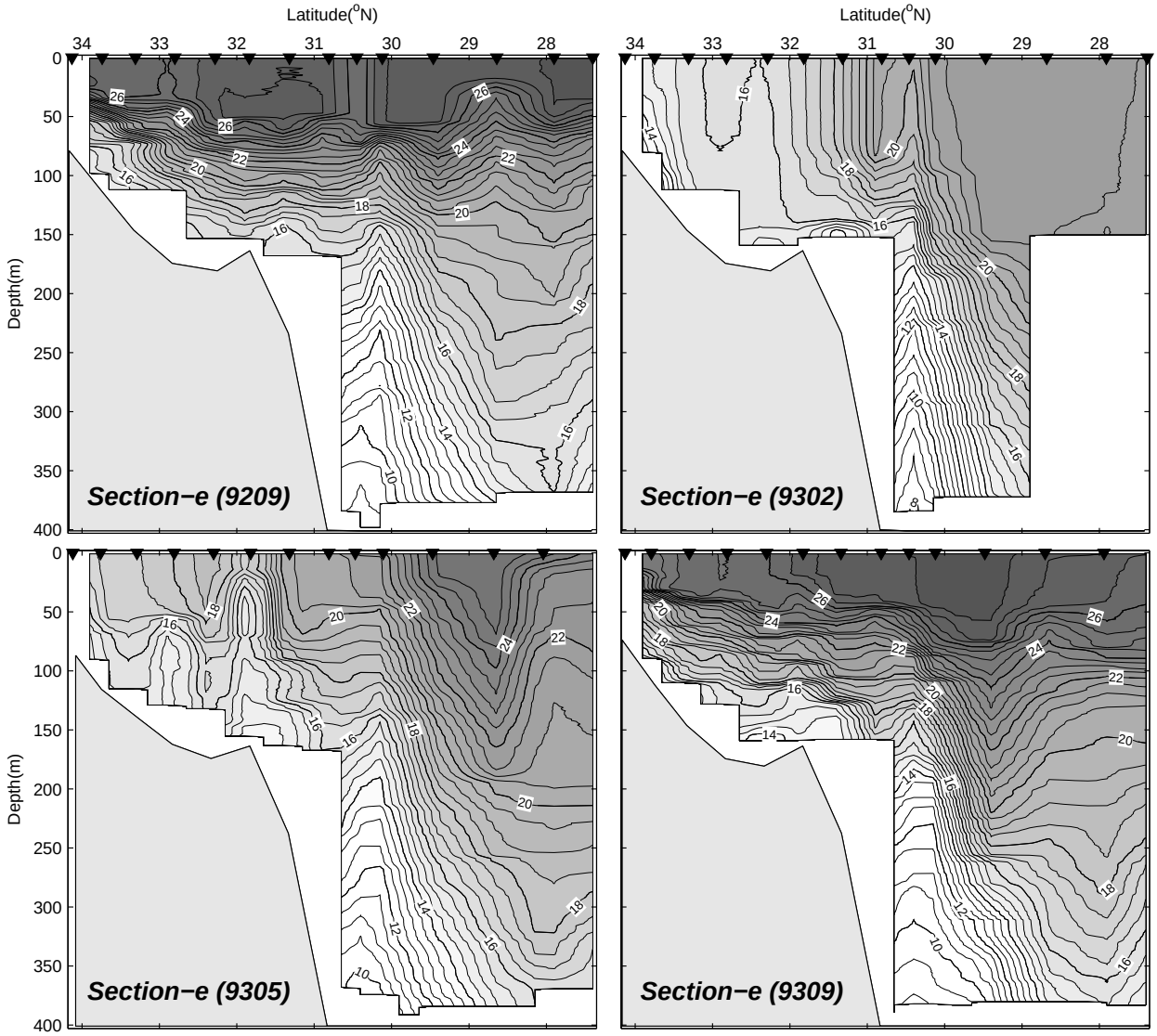

Figure 10. As Fig. 6 except for section-e.

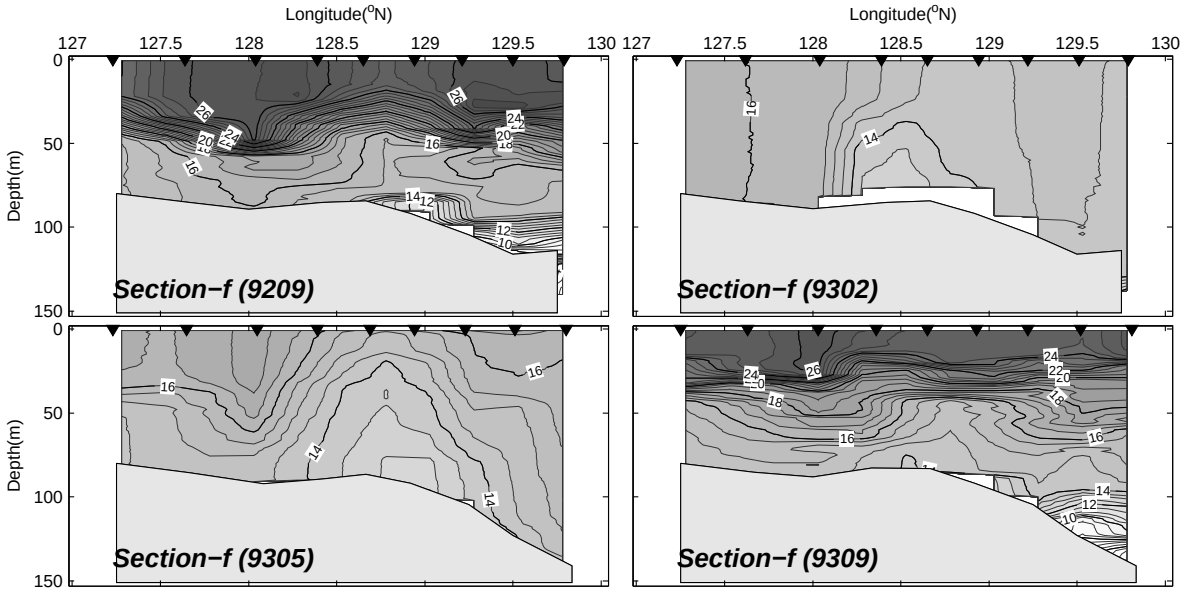

Figure 11. As Fig. 6 except for section-f.

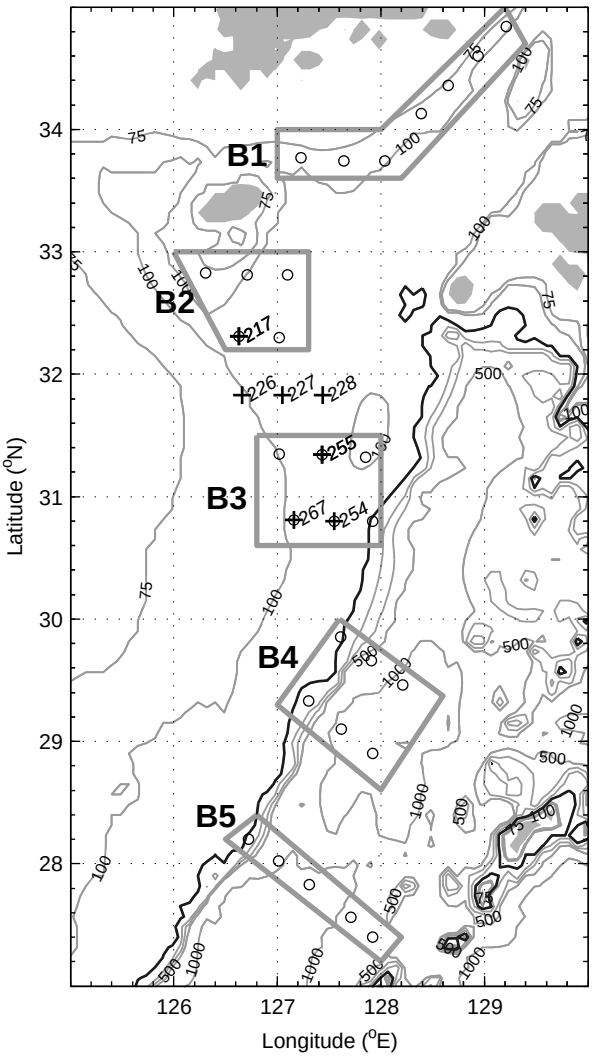

Figure 12. AXBT stations for calculating vertically-averaged variance of vertical temperature gradient, cross-frontal temperature gradient, heat flux, and eddy diffusivity. Five grey boxes are labeled by B1 (CTF), B2 (south of Cheju), B3 (CYF/TF), B4 (TF branching), and B5 (KF). Box-averaged estimates of the four parameters are listed in Table 1, and estimates of the parameters for individual stations marked with crosses and numbers in Table 2.